

COBEM-2017-2861

MECHANICAL BEHAVIOR OF ELASTOMERS UNDER UNIAXIAL TENSILE TESTS ASSISTED BY DIGITAL IMAGE TRACKING

Henrique Ossamu Hisano Natori

University of São Paulo, São Carlos School of Engineering, Department of Aeronautical Engineering
natori@usp.br

Katylín Rainara Cunha de Meira

Federal University of São Carlos (UFSCar), Materials Engineering Department (DEMa)
katylinmeira@outlook.com

Caiuã Caldeira de Melo

Federal University of São Carlos (UFSCar), Materials Engineering Department (DEMa), Postgraduate Program in Materials Science and Engineering (PPGCEM/UFSCar)
caiua.caldeira@gmail.com

Rodrigo Bresciani Canto

Federal University of São Carlos (UFSCar), Materials Engineering Department (DEMa)
rbcanto@ufscar.br

Ricardo Afonso Angélico

University of São Paulo, São Carlos School of Engineering, Department of Aeronautical Engineering
raa@sc.usp.br

Abstract. *The precise evaluation of parameters of material models is essential to achieve better design solutions, but conventional measuring techniques lead to difficulties when applied to materials that withstand large deformation, e.g. elastomers. Solutions as non-intrusive techniques have been developed to overcome these difficulties. The aim of the present article is to identify material model parameters from uniaxial tensile tests with subsequent loadings and unloadings assisted by digital image tracking (DIT). The identification procedure has been applied to four hyperelastic models: Neo-hookean, Arruda-Boyce, Mooney-Rivlin and Yeoh. A bicomponent translucent silicone rubber (RenCast 4644-1 - Huntsman) was studied under different displacement levels in order to observe the Mullins effect and evaluate parameters for the material model. Arruda-Boyce and Yeoh hyperelastic models with Mullins effect presented the best fit to the uniaxial tensile data.*

Keywords: *image tracking, elastomers, mechanical properties, hyperelastic model, Mullins effect*

1. INTRODUCTION

Elastomers are used in several applications due to their excellent energy absorption potential and their capacity to undergo large deformation and to retain initial configuration with small permanent strain after unloading. Vibration isolators, engine mounts and vehicles tires are some typical applications of this type of material (Kim *et al.*, 2004; Ilić *et al.*, 2017).

Several material models have been proposed to describe the behavior of elastomers, and, for large deformations, hyperelastic models are commonly used. Other phenomena such as Mullins effect and damage can also be included in these models. Some capacities are expected of an efficient hyperelastic material model as (Chagnon *et al.*, 2004):

- The ability to reproduce the 'S'-shaped response of elastomers;
- Behave under several deformation modes (tensile, pure shear, equibiaxial, etc.);
- A small number of parameters;
- A simple mathematical description suitable for numerical implementation.

Conventional measuring techniques lead to difficulties when applied to elastomers due to its large deformation. For

example, the contact of an extensometer on the specimen can influence the local mechanical behavior. Optical methods can overcome these difficulties by a non-intrusive evaluation of the displacement between two reference points, e.g. the digital image tracking (DIT). The aim of the present article is to identify the material model parameters from uniaxial tensile tests with subsequent loadings and unloadings, assisted by DIT.

2. HYPERELASTIC MATERIAL MODELS

Several review articles can be found about the constitutive relation for rubber materials (Boyce and Arruda, 2000; Marckmann and Verron, 2006). Due to their nonlinear behavior and large shape changes, they are modeled as hyperelastic materials. Hyperelastic models are described in terms of their strain energy potential, which is the energy stored per unit of reference volume when deforming it to the current configuration. Several models for this potential are proposed in the literature, and most of them describe it as a function of strain invariants (Dassault Systèmes Simulia, 2014). Hyperelastic material models can be written based on a phenomenological description, statistical mechanics or a combination of them.

One of the available models in AbaqusTM has a polynomial form, defined as:

$$U = \sum_{i+j=1}^N C_{ij}(\bar{I}_1 - 3)^i(\bar{I}_2 - 3)^j + \sum_{i=1}^N \frac{1}{D_i}(J_{el} - 1)^{2i} \quad (1)$$

where C_{ij} and D_i are material parameters, J_{el} is the elastic volume ratio, \bar{I}_1 and \bar{I}_2 are the first and second invariants of the left Cauchy-Green strain tensor, which are written in function of the stretch (λ), i.e.:

$$\bar{I}_1 = \bar{\lambda}_1^2 + \bar{\lambda}_2^2 + \bar{\lambda}_3^2 \quad (2)$$

$$\bar{I}_2 = \frac{1}{\bar{\lambda}_1^2} + \frac{1}{\bar{\lambda}_2^2} + \frac{1}{\bar{\lambda}_3^2} \quad (3)$$

The parameters D_i determine the material compressibility. In this work the material is assumed to be incompressible, which leads to $D_i = 0$.

When setting specific coefficients values, particular forms may be obtained, as the Neo-Hookean (Treloar, 1944), Mooney-Rivlin (Mooney, 1940) and Yeoh (Yeoh, 1990) forms, respectively described by:

$$U = C_{10}(\bar{I}_1 - 3) \quad (4)$$

$$U = C_{10}(\bar{I}_1 - 3) + C_{01}(\bar{I}_2 - 3) \quad (5)$$

$$U = C_{10}(\bar{I}_1 - 3) + C_{20}(\bar{I}_1 - 3)^2 + C_{30}(\bar{I}_1 - 3)^3 \quad (6)$$

Besides these phenomenological models, statistical mechanics models have been proposed as well, e.g. the Arruda-Boyce one, which is based on an eight-chain representation of the rubber network structure (Arruda and Boyce, 1993), resulting in a strain energy density function of the form

$$U = \mu \sum_{i=1}^5 \frac{C_i}{\lambda_m^{2i-2}} (\bar{I}_1 - 3)^i \quad (7)$$

where μ and λ_m are material parameters and

$$C_1 = \frac{1}{2}, \quad C_2 = \frac{1}{20}, \quad C_3 = \frac{11}{1050}, \quad C_4 = \frac{19}{7000}, \quad C_5 = \frac{519}{673750} \quad (8)$$

The identification of the hyperelastic model parameters consists on determining the values of the material constants C_{10} , C_{20} , C_{30} and C_{01} (for the models described in the Eqs. 4 - 6) and (μ, λ_m) for the Arruda-Boyce model (Eq. 7).

2.1 Mullins effect

Some elastomers present an initial transient softening behavior when subjected to cyclic loading, known as Mullins effect (Mullins, 1948, 1969). After the first loading, a stress-softening is observed, but subsequent loadings may be necessary for the response stabilization. The softening appears again whenever a larger stretch is applied. As the maximum stretch increases, this effect is intensified. The stress-strain response of an elastomer presenting this behavior is illustrated in Figure 1 (Diani *et al.*, 2009).

In AbaqusTM, the stress-softening is modeled by adding a scalar variable η to the strain energy potential function, which represents the damage in the material (Dassault Systèmes Simulia, 2014). The modified energy potential function is described by:

$$U = (\bar{\lambda}_i, \eta) = \eta \tilde{U}_{dev}(\bar{\lambda}_i) + \Phi(\eta) + \tilde{U}_{vol}(J_{el}) \quad (9)$$

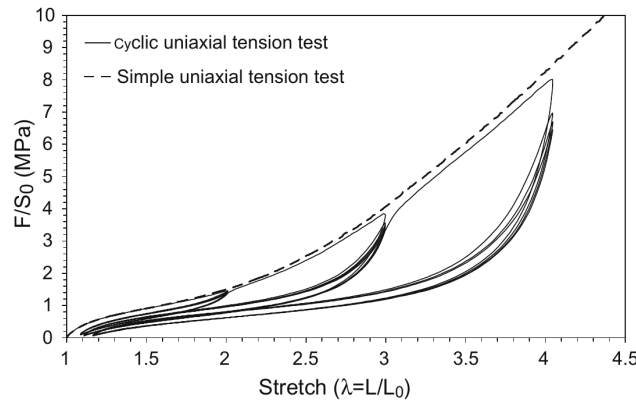


Figure 1. Softening behavior of elastomers presenting Mullins effect (Diani *et al.*, 2009).

where $\tilde{U}_{dev}(\bar{\lambda}_i)$ is the deviatoric part and $\tilde{U}_{vol}(J_{el})$ is the volumetric part of the strain energy potential of the monotonic hyperelastic behavior, which may be described by any of the previous energy functions. $\Phi(\eta)$ is the damage function, written in terms of η , which varies continuously and is expressed as:

$$\eta = 1 - \frac{1}{r} \operatorname{erf} \left(\frac{U_{dev}^m - \tilde{U}_{dev}}{m + \beta U_{dev}^m} \right) \quad (10)$$

where U_{dev}^m is the maximum value of \tilde{U}_{dev} during deformation history; r , β and m are material parameters; and $\operatorname{erf}(x)$ is the error function.

3. EXPERIMENTAL PROCEDURE

3.1 Material and specimens manufacturing

The specimens used in the mechanical tests were made of a room-temperature-vulcanization (RTV) silicone rubber (RenCast 4644-1 - Huntsman). It is produced by mixing the uncured silicone and the catalyst and curing it at room temperature. The mixture is molded into sheets with constant thickness, from which the test specimens are cut. The specimens manufacturing consists of five steps: (i) mixing the components with a 10/1 mass ratio (uncured silicone and catalyst, respectively); (ii) sheet molding ; (iii) inserting the mold in a vacuum chamber to reduce the presence of entrapped air bubbles; (iv) sheet demolding and specimens cutting; (v) marking dots on the specimens surface, used for the identification of the displacement by DIT. The dog-bone specimens were cut using a stamping jig (ISO 527 - specimen type 5A) and they had a section area of $4 \times 4 \text{ mm}^2$ and a 20 mm useful length.

3.2 Mechanical tests

Uniaxial tensile tests were conducted in a MTS-Bionix Universal Servo-hydraulic Testing Machine with a 5 kN capacity load cell. The specimens were subjected to subsequent loadings and unloadings at four different displacement levels, which increased progressively. Photographs were taken during each cycle.

The photographs were taken at 0.25 Hz with a CANON EOS Rebel T5 camera (18 megapixels sensor), a CANON EF 100 mm f/2.8 Macro lens and a LED lighting system. Figure 2 presents the experimental setup of the tensile tests.

3.3 Identification of the displacement by digital image tracking

The identification procedure consisted of five steps, illustrated in Figure 3: (a) a region of interest was selected and the images recorded during the test were cropped; (b) the information from the green layer of the images was filtered, as it presented better contrast; (c) an averaging filter was applied using the functions *fspecial* and *imfilter* available in MATLAB; (d) another filter was applied to create binary images; (e) finally, the centroids of the dots marked on the specimens were identified using the function *regionprops* in MATLAB. Maximum and minimum area criteria were adopted, besides restricting the search region to the center of the specimen. From the positions of the identified centroids in each image, their displacements were calculated and set as boundary conditions in the finite element model used for the identification of the hyperelastic model parameters.

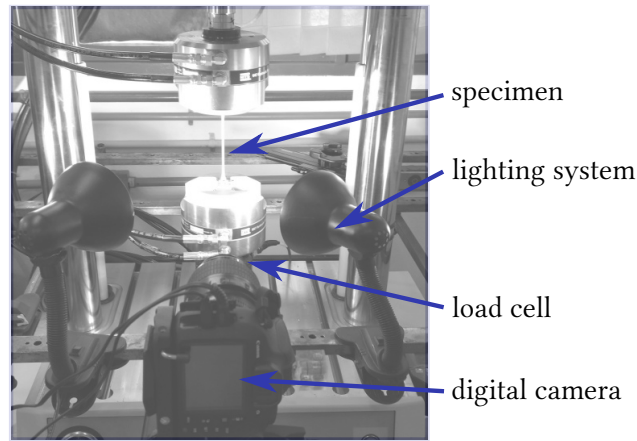


Figure 2. Experimental setup of the uniaxial tensile test assisted by digital image camera.

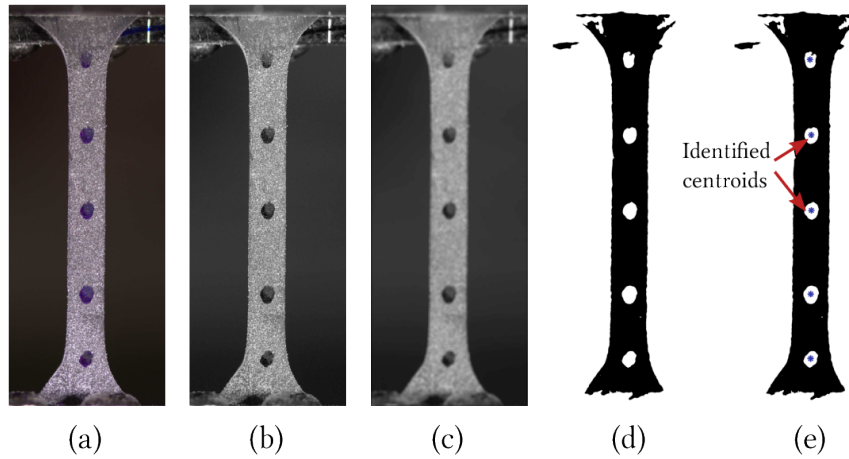


Figure 3. Procedure adopted for the identification of displacements. Steps: (a) original image; (b) green layer filtered image; (c) moving average filter; (d) binary operator over image; (e) identification of the centroids.

4. IDENTIFICATION PROCEDURE

The identification procedure of the hyperelastic model parameters was conducted by the comparison between the experimental and numerical data. This procedure is an iterative process that aims to identify the set of parameters (\mathbf{p}) that minimizes the quadratic difference (\mathcal{T}) between the axial load predicted by the finite element model ($F_{fem}(t, \mathbf{p})$) and the experimentally observed one ($F_{exp}(t)$), i.e.:

$$\mathcal{T}(\mathbf{p}) = \frac{1}{2} \int_0^{t_f} [F_{exp}(t) - F_{fem}(t, \mathbf{p})]^2 dt, \quad (11)$$

where t_f is the maximum testing time. The identification procedure has been conducted using Trust Region Reflective Algorithm through the function *lsqcurvefit* available in MATLAB.

The finite element model simulates the mechanical behavior of the elastomer under uniaxial tensile loading. Figure 4 presents an schema of the finite element model used in the identification process. The model considers a planar stress state where the inferior edge (A) has its vertical displacement constrained and in the superior edge (B), it is imposed the difference between the superior and inferior edges' displacements identified experimentally by the centroids position, $u_B - u_A$ (see Figure 3).

The identification procedure described above has been developed in two steps: (i) identification of hyperelastic model parameters and (ii) identification of Mullins effect parameters. In the first step, the experimental curve without the unloading has been used to identify the constitutive parameters (p_{hyper}). In the second step, the parameters identified before were fixed and the Mullins model parameters were identified $p_{mullins}$ using the complete experimental data (with unloadings). Table 1 presents the parameters to be identified in each procedure.

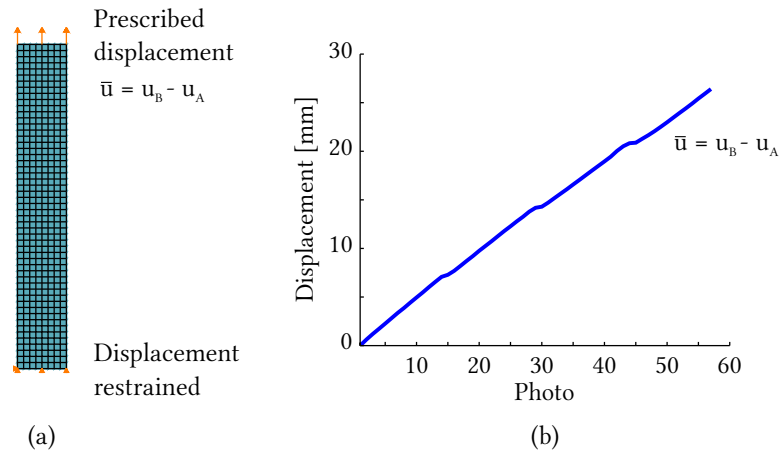


Figure 4. Finite element model used in the identification procedure.

Table 1. Parameters of interest to be identified.

Identification step	Hyperelastic model	Parameters
(i) Hyperelastic parameters	Neo-hookean (NH)	$p_{hyper} = [C_{10}]$
	Arruda-Boyce (AB)	$p_{hyper} = [\mu \quad \lambda_m]$
	Money-Rivlin (MR)	$p_{hyper} = [C_{10} \quad C_{01}]$
	Yeoh (Y)	$p_{hyper} = [C_{10} \quad C_{20} \quad C_{30}]$
(ii) Mullins model parameters	ALL*	$p_{mullins} = [r \quad m \quad \beta]^T$

5. RESULTS AND DISCUSSION

The first part of the identification procedure was conducted to compute the hyperelastic model parameters using the experimental curves without the unloadings. Table 2 presents the identified parameters for Neo-hookean, Arruda-Boyce, Money-Rivlin and Yeoh hyperelastic models. Figure 5 shows the comparison of the identified models and the experimental data used in the identification procedure. Based on the identification residual, \mathcal{T} (eq. (11)), the best model fit was obtained using Arruda-Boyce and Yeoh hyperelastic models. For these models, the largest identification residuals were observed for the stretch between 1.7 and 1.8. The models are in good agreement with the experimental results, however, it can be seen that the stress is overestimated up to stretch 1.4 and underestimated from 1.4 up to 1.75. This behavior shows that the model can be used for engineering purposes only. Although the Mooney-Rivlin model also presents a good fit, the negative C_{01} parameter identified may lead to unstable behavior for different loading modes (Bergström, 2015, p. 243).

Table 2. Identified parameters for different hyperelastic models based on the monotonic loading.

Hyperelastic model	Identified parameters
Neo-hookean (NH)	$C_{10} = 1.317$
Arruda-Boyce (AB)	$\mu = 0.8313, \lambda_m = 1.161$
Money-Rivlin (MR)	$C_{10} = 3.129, C_{01} = -2.872$
Yeoh (Y)	$C_{10} = 1.028, C_{20} = 0.0000, C_{30} = 0.1075$

The identified Arruda-Boyce and Yeoh models were used in the second part of the identification procedure to describe the primary hyperelastic behavior, and Mullins model parameters were computed for each case using the experimental curves with the unloadings. Table 3 presents the identified parameters using each hyperelastic model. Figures 6 and 7 show the comparison of the response considering and not considering Mullins effect and the experimental data used.

Table 3. Mullins model parameters identified for Arruda-Boyce and Yeoh hyperelastic models.

Hyperelastic model	Identified parameters
Arruda-Boyce (AB+M)	$r = 2.061, m = 0.3342, \beta = 0.1771$
Yeoh (Y+M)	$r = 1.983, m = 0.2349, \beta = 0.2763$

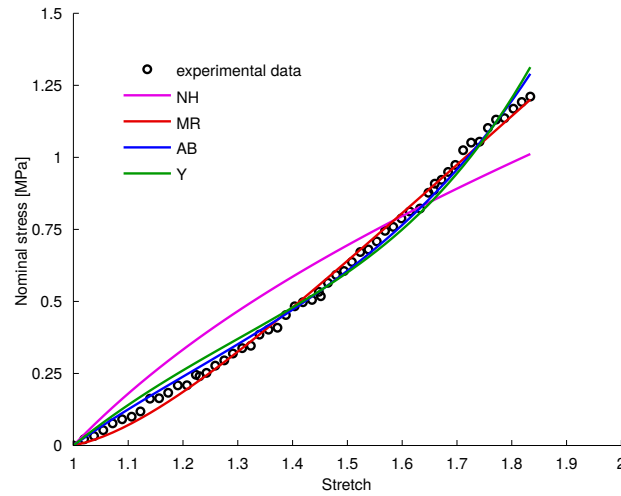


Figure 5. Comparison between experimental data and the identified hyperelastic models. Arruda-Boyce and Yeoh presented the lower residual in the identification procedure.

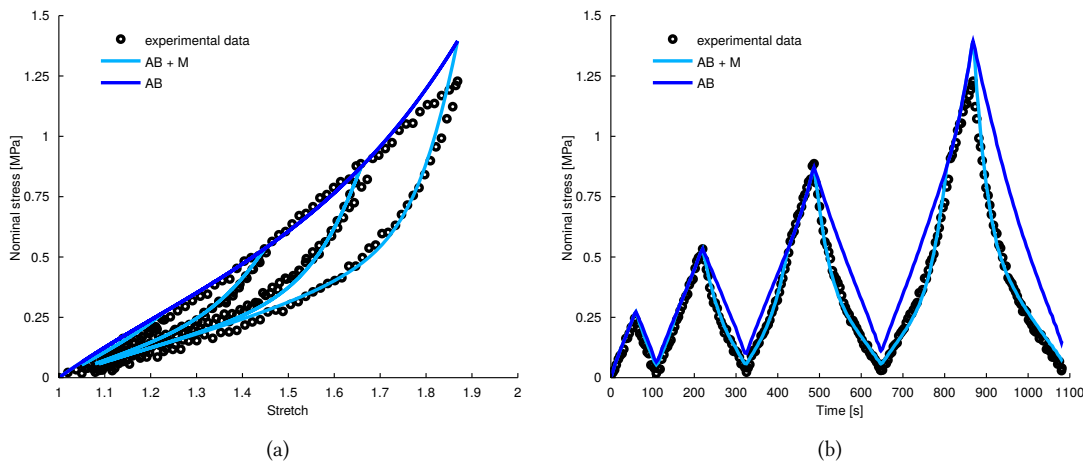


Figure 6. Hyperelastic response according to Arruda-Boyce hyperelastic model with and without Mullins effect: (a) stress vs. strain response; (b) stress vs. time response.

The results presented herein are preliminary and other tests – with more complex stress states – are necessary. Only with these new tests, it will be possible to attest that the identified parameters have a physical significance. More robust displacement measurements techniques, like Digital Image Correlation (DIC), will enable to capture different stress states in a single test. However, some challenges must be overcome to apply this technique in specimens that undergo large deformations, which can take off the artificial texture over the specimen during the tests, for example.

The studied hyperelastic models are able to predict the mechanical behavior of the elastomer under uniaxial loading and also the softening behavior when applying the Mullins model. The investigation of the material response under different deformation modes, though, is required to obtain a more suitable model for engineering applications.

6. CONCLUSIONS

The mechanical behavior under uniaxial loading of a bicomponent silicone rubber has been identified using an image tracking algorithm, that enabled to measure the specimens' strain, showing to be a valuable tool for identification of the hyperelastic models parameters. It is important to highlight that because of the rubber flexibility, it is difficult to adopt sensors, like strain gauges, to measure its behavior. Hyperelastic models parameters have been identified and the Arruda-Boyce and Yeoh ones presented the best fit to the experimental behavior without unloadings. The unloading behavior can be only fit by the introduction of the Mullins effect into the model, which can be described by three parameters. These were also identified for each of the best fit models. A good agreement between the fit models and the experimental data could be observed (maximum difference between experimental and numerical prediction of 0.15 MPa was obtained), but improvements can be achieved by conducting other experiments involving different kinds of stress states (e.g. planar, pure

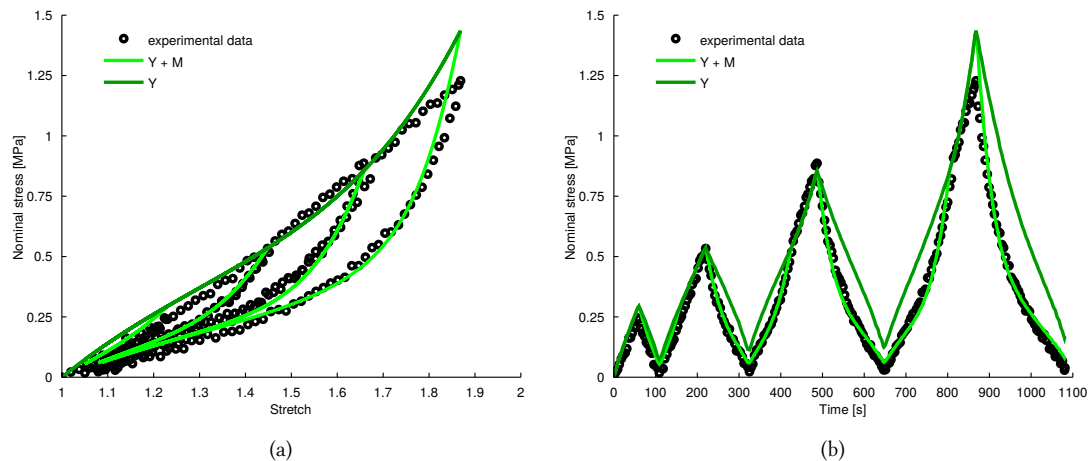


Figure 7. Hyperelastic response according to Yeoh hyperelastic model with and without Mullins effect: (a) stress vs. strain response; (b) stress vs. time response.

shear, equibiaxial).

7. ACKNOWLEDGEMENTS

The authors would like to thank CNPq (Proc. 164746/2017-0) for the financial support. Also, we would like to thank Elisa Gamper Vergamini for her valuable assistance during the experimental tests.

8. REFERENCES

- Arruda, E.M. and Boyce, M.C., 1993. "A three-dimensional constitutive model for the large stretch behavior of rubber elastic materials". *Journal of the Mechanics and Physics of Solids*, Vol. 41, No. 2, pp. 389–412. ISSN 00225096. doi:10.1016/0022-5096(93)90013-6.
- Bergström, J., 2015. *Mechanics of solid polymers : theory and computational modeling*. ISBN 9780323311502.
- Boyce, M.C. and Arruda, E.M., 2000. "Constitutive Models of Rubber Elasticity: A Review". *Rubber Chemistry and Technology*, Vol. 73, No. 3, pp. 504–523. ISSN 0035-9475. doi:10.5254/1.3547602.
- Chagnon, G., Marckmann, G. and Verron, E., 2004. "A comparison of the hart-smith model with arruda-boyce and gent formulations for rubber elasticity". *Rubber chemistry and technology*, Vol. 77, No. 4, pp. 724–735. ISSN 0035-9475. doi:10.5254/1.3547847.
- Dassault Systèmes Simulia, 2014. *Abaqus 6.14 Theory Guide*. ISBN 9788578110796. doi:10.1017/CBO9781107415324.004.
- Diani, J., Fayolle, B. and Gilormini, P., 2009. "A review on the Mullins effect". *European Polymer Journal*, Vol. 45, No. 3, pp. 601–612. ISSN 00143057. doi:10.1016/j.eurpolymj.2008.11.017.
- Ilić, Z., Rašuo, B., Jovanović, M., Jovičić, S., Tomić, L., Janković, M. and Petrašinović, D., 2017. "The efficiency of passive vibration damping on the pilot seat of piston propeller aircraft". *Measurement*, Vol. 95, pp. 21–32. ISSN 02632241. doi:10.1016/j.measurement.2016.09.042.
- Kim, W., Lee, H., Kim, J. and Koh, S.K., 2004. "Fatigue life estimation of an engine rubber mount". *International Journal of Fatigue*, Vol. 26, No. 5, pp. 553–560. ISSN 01421123. doi:10.1016/j.ijfatigue.2003.08.025.
- Marckmann, G. and Verron, E., 2006. "Comparison of Hyperelastic Models for Rubber-Like Materials". *Rubber Chemistry and Technology*, Vol. 79, No. 5, pp. 835–858. ISSN 0035-9475. doi:10.5254/1.3547969.
- Mooney, M., 1940. "A Theory of Large Elastic Deformation". *Journal of Applied Physics*, Vol. 11, No. 9, pp. 582–592. ISSN 0021-8979. doi:10.1063/1.1712836.
- Mullins, L., 1948. "Effect of Stretching on the Properties of Rubber". *Rubber Chemistry and Technology*, Vol. 21, No. 2, pp. 281–300. ISSN 0035-9475. doi:10.5254/1.3546914.
- Mullins, L., 1969. "Softening of Rubber by Deformation". *Rubber Chemistry and Technology*, Vol. 42, No. 1, pp. 339–362. ISSN 0035-9475. doi:10.5254/1.3539210.
- Treloar, L.R.G., 1944. "The Elasticity of a Network of Long-Chain Molecules. II". *Rubber Chemistry and Technology*, Vol. 17, No. 2, pp. 296–302. ISSN 0035-9475. doi:10.5254/1.3546653.
- Yeoh, O.H., 1990. "Characterization of Elastic Properties of Carbon-Black-Filled Rubber Vulcanizates". doi:10.5254/1.3538289.

9. RESPONSIBILITY NOTICE

The authors are the only responsible for the printed material included in this paper.